

Modified weak-value-amplification technique for measuring a mirror's velocity based on the Vernier effect

Jing-Hui Huang ^{1,2,*} Fei-Fan He ^{1,†} Xue-Ying Duan ^{3,4,2,‡} Guang-Jun Wang ^{3,4,2,§} and Xiang-Yun Hu ^{1,2,||}

¹*Institute of Geophysics and Geomatics, China University of Geosciences, Lumo Road 388, 430074 Wuhan, China*

²*Engineering Research Center of Intelligent Technology for Geo-Exploration, Ministry of Education, 430074 Wuhan, China*

³*School of Automation, China University of Geosciences, Lumo Road 388, 430074 Wuhan, China*

⁴*Hubei Key Laboratory of Advanced Control and Intelligent Automation for Complex Systems, 430074 Wuhan, China*



(Received 17 August 2021; accepted 11 January 2022; published 27 January 2022)

A modified weak-value-amplification (MWVA) technique to measure a mirror's velocity based on the Vernier effect is proposed. To demonstrate its enhanced sensitivity and higher signal-to-noise ratio (SNR), we use two cascaded Michelson interferometers with similar optical structures. One has a fixed mirror and acts as a fixed part of the Vernier scale, while the other, with a moving mirror, acts as a sliding part of the Vernier scale for velocity sensing. The envelope of the cascaded interferometers shifts much more than a single one with a certain enhancement factor, which is related to the free space range difference between them. In addition, we calculate the SNR based on the Fisher information with both the MWVA and traditional weak-value-amplification (TWVA) techniques. The results show that both the SNR and the sensitivity with our MWVA technique is greater than that of the TWVA technique within the range of our time measurement window. In particular, MWVA can present a viable and effective alternative to the TWVA technique out of the limit of resolution. Furthermore, by using the principles of the Vernier effect, it is applicable and convenient to improve the sensitivity and SNR in measuring other quantities with the TWVA technique.

DOI: [10.1103/PhysRevA.105.013718](https://doi.org/10.1103/PhysRevA.105.013718)

I. INTRODUCTION

Weak measurement is a new tool in quantum mechanics to characterize postselected quantum systems [1,2], first proposed by Aharonov, Albert, and Vaidman [3] as an extension to the standard (projective) von Neumann model of measurement. In weak measurement, information is gained by weakly probing the system while approximately preserving its initial state. The average shift of the final pointer state can go far beyond the eigenvalue spectrum of the system, in sharp contrast with the standard quantum measurement. This average shift is called the weak value and is usually complex [4–6]. These features are widely applicable to understand many counterintuitive quantum results, offering new insights into paradoxes, such as Hardy's paradox [7–9], the three-box paradox [10,11], apparent superluminal travel [12], and the direct measurement of the real and imaginary components of the wave function [13].

In addition to the fundamental physical interest in weak values, a major goal in weak measurement is to enhance sensitivity when estimating weak signals [14–18]. Dixon *et al.* amplified very small transverse deflections of an optical beam, then measured the angular deflection of a mirror down to

400 ± 200 frad, and the linear travel of a piezo actuator down to 14 ± 7 fm [19]. Boyd *et al.* first realized weak-value amplification in the azimuthal degree of freedom, and achieved effective amplification factors as large as 100 [15]. Viza *et al.* achieved a velocity measurement of 400 fm/s by measuring the Doppler shift due to a moving mirror in a Michelson interferometer [20]. Pati *et al.* proposed an alternative method to measure the temperature of a bath using the weak measurement scheme with a finite-dimensional meter [21]. These applications are known in the literature as weak-value-amplification (WVA) techniques [22].

It is worth noting that weak-value-amplification cannot be arbitrarily large with decreasing output laser intensity [23]. Koike *et al.* [24] showed that the measured displacement and amplification factor are not proportional to the weak value and vanish in the limit of infinitesimal output intensity. Pang *et al.* [25] investigated the limiting case of continuous-variable systems to demonstrate the influence of system dimension on the amplification limit. It is still the focus in weak measurement to enhance the sensitivity of detecting small signals. Starling *et al.* [26] and Feizpour *et al.* [27] showed that postselection can significantly raise the signal-to-noise ratio (SNR) of weak measurement. Huang *et al.* [28] proposed dual weak-value amplification (DWVA), with sensitivity several orders of magnitude higher than the standard approach, without losing signal intensity. Krafczyk *et al.* [29] experimentally demonstrated recycled weak-value measurements by using photon counting detectors to improve the signal by a factor of 4.4 ± 0.2 and improving the SNR by 2.1 ± 0.06 compared with a single-pass weak-value experiment. In addition, there

*jinghuihuang@cug.edu.cn

†hfeifan2017@cug.edu.cn

‡CUGxyDuan@163.com

§gjwang@cug.edu.cn

||Corresponding author: xyhu@cug.edu.cn

has been a strong interest in applying conditional measurements in which photon statistics (photon-number operators) is employed as the measuring device [30–32].

The Vernier effect has been effective at enhancing the sensitivity of photonic devices [33–36]. It is an efficient method to enhance the accuracy of measurement instruments, and consists of two or three scales with different periods. A sensor consisting of two cascaded ring resonators was shown theoretically to attain very high sensitivity thanks to the Vernier principle [33]. A high sensitivity of 1892 dB/RIU of an optical sensor was achieved for intensity interrogation based on cascaded reflective Mach-Zehnder interferometers (MZI) and microring resonators [35]. A refractive index optical sensor based on three cascaded microring resonators had a high sensitivity of 5866 nm/RIU, whose measurement range was significantly improved 24.7 times compared with the traditional two cascaded microring resonators [36].

We propose modified weak-value amplification (MWVA) with two cascaded Michelson interferometers to improve the sensitivity of traditional weak-value amplification (TWVA) based on the Vernier effect. Specifically, in the framework of quantum weak measurements, we observe the temporal shift induced by a small spectral shift with two cascaded Michelson interferometers. The spectral shift in our scheme is a Doppler frequency shift produced by a mirror in one of the interferometers, while the other interferometer has the same optical structure with no movement of the mirror. By numerical simulation, we obtain the temporal shift dependence of the velocity, sensitivity, and SNR calculated from the Fisher information [37]. MWVA is comparable to TWVA, but it allows us to reach a higher sensitivity and SNR under the same conditions of measuring time.

The rest of this paper is organized as follows. Section II A briefly reviews the TWVA technique for measuring velocity in a single Michelson interferometer. In Sec. II B, we derive the MWVA technique for velocity with two cascaded Michelson interferometers based on the Vernier effect. In Sec. III, by ensuring the same time measurement window and determining the meters in the two techniques, we obtain analytic results of the sensitivity and SNR from the Fisher information. Section IV consists of the summary and discussion.

II. TRADITIONAL WEAK-VALUE-AMPLIFICATION AND MODIFIED WEAK-VALUE-AMPLIFICATION TECHNIQUES

We propose and numerically demonstrate a weak measurement scheme, in which the amplification of the phase shifts in a Michelson interferometer can be effectively enhanced by introducing another cascaded interferometer based on the Vernier effect.

A. Weak-value-amplification technique for velocity measurement

We review the traditional WVA technique to measure velocity with a Michelson interferometer [20]. The temporal shift is proportional to the weak value and can be amplified in the measurement of v , which is accompanied by a decrease in the measured intensity due to the nature of the weak

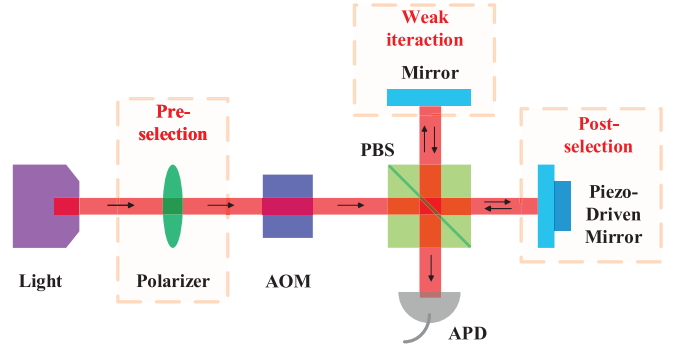


FIG. 1. Schematic of WVA technique for velocity measurement in the single Michelson. AOM is the acousto-optic modulator, which can modulate the light into a temporal Gaussian-shaped pulse. PBS is the polarizer beam splitter. The arrival time of single photons is measured with an avalanche photodiode (APD).

measurement. The temporal shift is induced by the spectral shift, which is a Doppler frequency shift produced by a moving mirror in a Michelson interferometer. The WVA technique for velocity measurement is shown in Fig. 1.

In principle, the TWVA technique of weak measurement has three parts: state preparation, weak interaction, and post-selection. The initial state $|\Phi_i\rangle$ of the system and $|\Psi_i\rangle$ of the meter are prepared with the polarizer and AO modulator. The initial polarization state of the system can be described by the polarization qubit,

$$|\Phi_i\rangle = \sin(\alpha)|H\rangle + \cos(\alpha)|V\rangle, \quad (1)$$

where $\alpha = \pi/4$ rad is the angle between the horizontal line and the transmission axis of the line polarizer (preselection). The horizontal polarization state $|H\rangle$ corresponds to the arm with the mirror through which the light passes, and the vertical polarization state $|V\rangle$ to the arm with the piezo-driven mirror in the Michelson interferometer. The preparation of the meter consists of the generation of the temporal mode,

$$I_{\text{single}}^i = |\langle p|\Psi_i\rangle|^2(t) = I_0 \frac{1}{\sqrt{2\pi}\tau^2} e^{-(t+t_0)^2/2\tau^2}, \quad (2)$$

where τ is the length of the Gaussian pulse, t_0 is the center of the pulse, and the value of I_0 is normalized to 1. The advantage of the temporal meter and non-Fourier limited Gaussian-shaped pulse has been studied [20]. The pulse is injected into a Michelson interferometer, where the horizontally polarized component of the pulse goes through the arm with a slowly moving mirror at speed v , and the vertically polarized component goes through the arm with a piezo-driven mirror. The weak interaction in Fig. 1 can be expressed as

$$U = e^{-ig\hat{A}\otimes\hat{p}} = e^{-i\omega_d\hat{A}t/2}, \quad (3)$$

where $\omega_d = 2\pi f_d = 2\pi \frac{2v}{\lambda}$. Note that the spectral shift $f_d = 2v/\lambda$ is proportional to the velocity v . The observable \hat{A} satisfies $\hat{A} = |H\rangle\langle H| - |V\rangle\langle V|$.

The postselection of the weak measurement is controlled by inducing a phase offset 2ϕ by the piezo-driven mirror. Thus, the final postselection of the system is

$$|\Phi_f\rangle = \frac{1}{\sqrt{2}}(|H\rangle - e^{i2\phi}|V\rangle), \quad (4)$$

and the weak value is

$$A_w = \frac{\langle \Phi_f | \hat{A} | \Phi_i \rangle}{\langle \Phi_f | \Phi_i \rangle} = -i \cot \phi \approx \frac{-i}{\phi}. \quad (5)$$

The meter state of the temporal mode after the postselection becomes [3]

$$\begin{aligned} \langle p | \Psi_f \rangle &= \langle \Phi_f | U | \Phi_i \rangle \langle p | \Psi_i \rangle \\ &= \langle \Phi_f | e^{-ig\hat{A} \otimes \hat{p}} | \Phi_i \rangle \langle p | \Psi_i \rangle \\ &= \langle \Phi_f | \Phi_i \rangle [1 - igA_w \hat{p}] \langle p | \Psi_i \rangle + O(g^2) \\ &\approx \langle \Phi_f | \Phi_i \rangle e^{-igA_w \hat{p}} \langle p | \Psi_i \rangle. \end{aligned} \quad (6)$$

Hence, the squared absolute value of the meter state (6) is

$$\begin{aligned} I_{\text{single}}^f &= |\langle p | \Psi_f \rangle|^2 \\ &= (\sin \phi)^2 e^{-\frac{4\pi v t}{\lambda \phi}} |\langle p | \Psi_i \rangle|^2 \\ &= \frac{(\sin \phi)^2}{\sqrt{2\pi \tau^2}} e^{-\frac{4\pi v t}{\lambda \phi}} e^{-(t+t_0)^2/2\tau^2} \\ &\approx \frac{(\sin \phi)^2}{\sqrt{2\pi \tau^2}} e^{-\left(t+t_0 + \frac{4\pi \tau^2 v}{\lambda \phi}\right)^2/2\tau^2}. \end{aligned} \quad (7)$$

The final step of Eq. (7) is obtained by assuming

$$\frac{(4\pi \tau^2 v)^2}{2\tau^2 (\lambda \phi)^2} = \frac{4\pi \tau^2 v}{\lambda \phi} \frac{2\pi v}{\lambda \phi} = \frac{\delta t}{\tau} \frac{2\pi v \tau}{\lambda \phi} \ll 1, \quad (8)$$

where the condition $2\pi v \tau \ll \lambda \phi$ is consistent with the Ref. [20] and the relationship $\delta t < \tau$ is nature in the working range of the weak measurement. In the traditional WVA technique to measure velocity, the time shift $\delta t = \frac{4\pi \tau^2 v}{\lambda \phi}$ in Eq. (7) is amplified in the measurement of v . Note that the spectral shift $f_d = 2v/\lambda$ can translate to the time shift $\delta t = \frac{2\pi \tau^2 f_d}{\phi} = \frac{4\pi \tau^2 v}{\lambda \phi}$ [20].

In addition, we show the time shift of the meter in the scheme of the TWVA technique to measure velocity $v = 30$ nm/s with length $\tau = 0.2$ ms and central wavelength $\lambda = 800$ nm of the Gaussian pulse in Fig. 2. An interferometric scheme based on a purely imaginary weak value was studied, combined with a frequency-domain analysis, perhaps with the potential to outperform standard interferometry by several orders of magnitude [38]. However, the amplification of the TWVA technique cannot be arbitrarily large due to the limit of the resolution of the detector.

B. Modified weak-value-amplification technique based on Vernier effect

Figure 3 shows the schematic diagram of the MWVA technique for measuring velocity. It includes two Michelson interferometers based on the TWVA technique, which are the same as with the TWVA technique in Fig. 1. The upper interferometer with moving mirror 1 serves as the sliding part of the Vernier scalar because velocity changes will cause a shift of the final meter. The lower interferometer with static mirror 2 serves as the fixed part. The Vernier scale, consisting of two scales with different periods, can efficiently enhance the accuracy of measurement instruments [39].

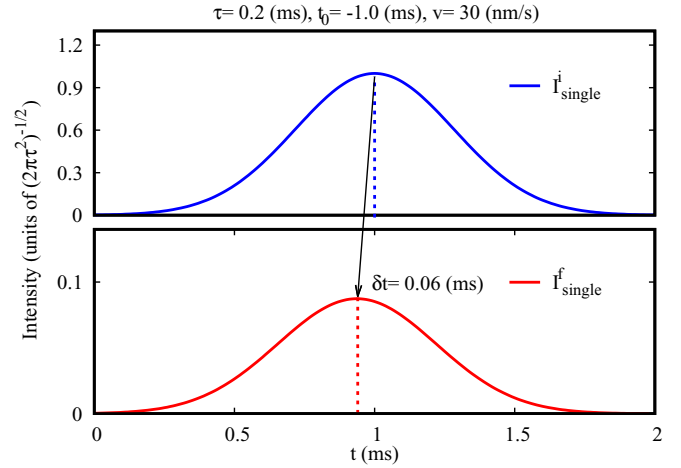


FIG. 2. Time shift of meter in the scheme of the WVA technique to measure velocity $v = 30$ nm/s with length of Gaussian pulse $\tau = 0.2$ ms and phase offset $\phi = 0.3$ rad of postselection. The vertical dotted line represents the corresponding center of the Gaussian function.

In our work, the upper and lower interferometers are prepared with different free spectrum ranges (FSRs). The total transmission meter of the cascaded Michelson interferometer is the superposition of the optical power output of two interferometers, which exhibits peaks when their interference peaks partially overlap. The envelope period is

$$\frac{\bar{R}_{\text{sliding}} \times \bar{R}_{\text{fixed}}}{|\bar{R}_{\text{sliding}} - \bar{R}_{\text{fixed}}|}. \quad (9)$$

When the velocity changes, the transmission of the single (upper) interferometer will shift, and the shift of the cascaded Michelson interferometers' envelope is magnified by the factor \bar{E} . The shift of the transmission peak is proportional to the

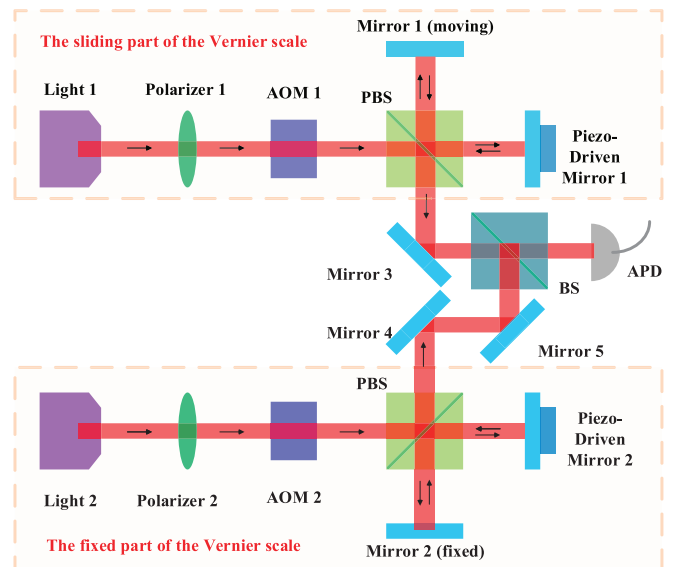


FIG. 3. Scheme of MWVA technique with two cascaded Michelson interferometers based on Vernier effect.

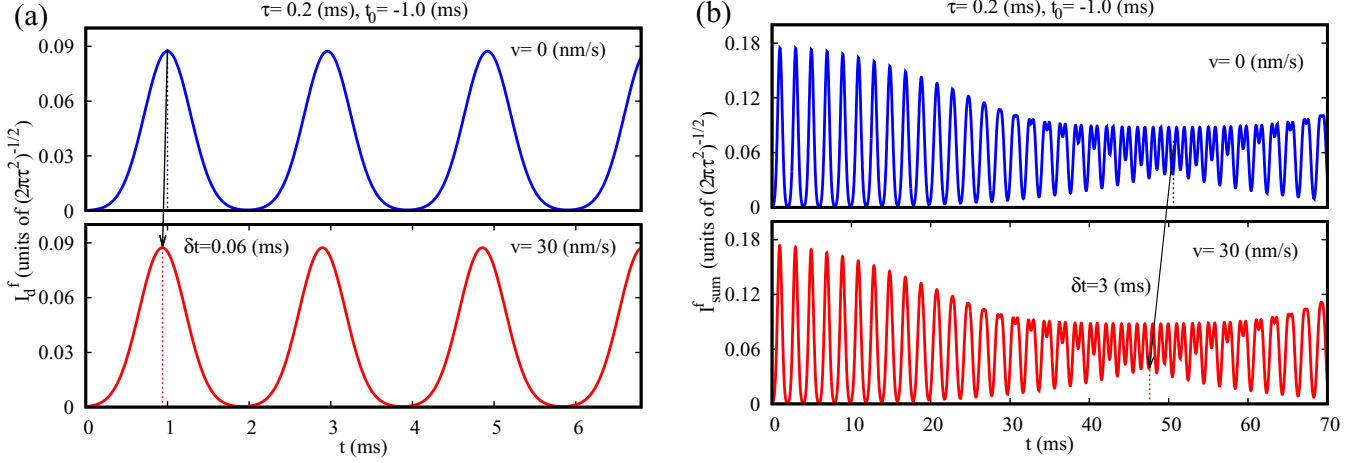


FIG. 4. Numerical simulation of the transmission temporal shift δt with $\tau = 0.2$ ms and $t_0 = -1.0$ ms at different velocity v . Panel (a) shows the final meter I_d^f of single Michelson interferometer, the upper plane (blue curve) represents the results measured at $v = 0.0$ nm/s and the lower plane (red curve) is corresponding to the signal measured at $v = 3.0$ nm/s. The temporal shift δt is calculated by fitting the shift of the peak of the two curves. Panel (b) displays the final meter I_{sum}^f of two cascaded Michelson interferometers. Similarly, the temporal shift δt is obtained from the shift of the envelope of the two curves. The units of the y coordinate of each graph is $(2\pi\tau^2)^{-1/2}$

enhanced factor,

$$\bar{E} = \frac{\bar{R}_{\text{fixed}}}{|\bar{R}_{\text{sliding}} - \bar{R}_{\text{fixed}}|}. \quad (10)$$

To produce the Vernier effect, the parameters of the main optical components in our scheme in Fig. 3 must meet the following requirements:

(i) *Light*: a high-power light source is suitable. Note that the pulses for lights 1 and 2 need not be coherent, because the laser detected at APD is the superposition of the optical power output of two interferometers.

(ii) *Piezo-driven mirror*: the postselection of the TWVA technique is controlled by inducing a phase offset 2ϕ with the piezo-driven mirror, i.e., the intensity of the outgoing light is proportional to the phase offset, as shown in Eq. (7). To obtain the overlap with easily discernible peaks, the intensity of the outgoing light of each interferometer, i.e., the phase offset, should keep the same value.

(iii) *AOM*: this is the most critical device. The pulse, which serves as the sliding or fixed part of the Vernier scale, should be produced with an equally spaced Gaussian mode rather than an individual pulse (2) [35,36,39]. AOM is mainly used outside the laser cavity and modulates the laser with the electric signal of the driving source [40]. In our work, AOM 1 modulates the laser with \bar{R}_{sliding} as the preselection meter $|\langle p|\Psi_i\rangle|_{\text{sliding}}^2 = I_u^i$ in the upper interferometer, while AOM 2 modulates the laser with \bar{R}_{fixed} as the preselection meter $|\langle p|\Psi_i\rangle|_{\text{fixed}}^2 = I_d^i$ in the lower interferometer. Then,

$$I_u^i = \sum_{m=0}^N \frac{1}{\sqrt{2\pi\tau^2}} e^{-(t+t_0-m\bar{R}_{\text{sliding}})^2/2\tau^2}, \quad (11)$$

$$I_d^i = \sum_{m=0}^N \frac{1}{\sqrt{2\pi\tau^2}} e^{-(t+t_0-m\bar{R}_{\text{fixed}})^2/2\tau^2}. \quad (12)$$

The final meter $|\langle p|\Psi_f\rangle|_{\text{fixed}}^2(t) = I_d^f$ of the lower interferometer becomes

$$I_d^f = \sum_{m=0}^N \frac{(\sin\phi)^2}{\sqrt{2\pi\tau^2}} e^{-(t+t_0-m\bar{R}_{\text{fixed}})^2/2\tau^2}. \quad (13)$$

The final meter $|\langle p|\Psi_f\rangle|_{\text{sliding}}^2(t) = I_u^f$ of the upper interferometer with moving mirror 1 at velocity v becomes

$$I_u^f = \sum_{m=0}^N \frac{(\sin\phi)^2}{\sqrt{2\pi\tau^2}} e^{-(t+t_0-m\bar{R}_{\text{sliding}}+\frac{4\pi\tau^2v}{\lambda\phi})^2/2\tau^2}. \quad (14)$$

The intensity of the total laser detected at APD is the sum of the light power from the upper and lower interferometers, i.e., $I_{\text{sum}}^f = I_u^f + I_d^f$.

We select an experimental setup with $\phi = 0.3$ rad, $\tau = 0.2$ ms, $\lambda = 800$ nm, $t_0 = 1.0$ ms of pulse I_u^i (11) and I_d^i (12), $\bar{R}_{\text{fixed}} = 2.0$ ms, and $\bar{R}_{\text{sliding}} = 1.96$ ms of the upper interferometer. The numerical simulations of the transmission temporal shift of a single Michelson interferometer and two cascaded Michelson interferometers are shown in Figs. 4(a) and 4(b), respectively. The sensitivity-enhanced factor $\bar{E} = \frac{3 \text{ ms}}{0.06 \text{ ms}} = 50$ due to the Vernier effect is the same as $\bar{E} = \frac{2.00 \text{ ms}}{2.00 \text{ ms} - 1.96 \text{ ms}} = 50$, calculated from Eq. (10). The results verify that the sensitivity for measuring velocity can be enhanced according to the calculated sensitivity-enhanced factor (10) by choosing two interferometers with smaller differences in FSR. However, in practice, there is a compromise between sensitivity and measurement accuracy because a smaller FSR difference will increase the FSR of the envelope, which introduces difficulty in tracking the temporal shift of the envelope peak [39].

The numerical results show that the MWVA technique based on the Vernier effect is more sensitive than the TWVA technique regardless of the measurement time of these two techniques. In the scheme of the TWVA technique, Eq. (7) indicates that the time shift $\delta t = \frac{4\pi\tau^2v}{\lambda\phi}$ can be effectively enhanced by increasing the measuring time. Figure 4 shows

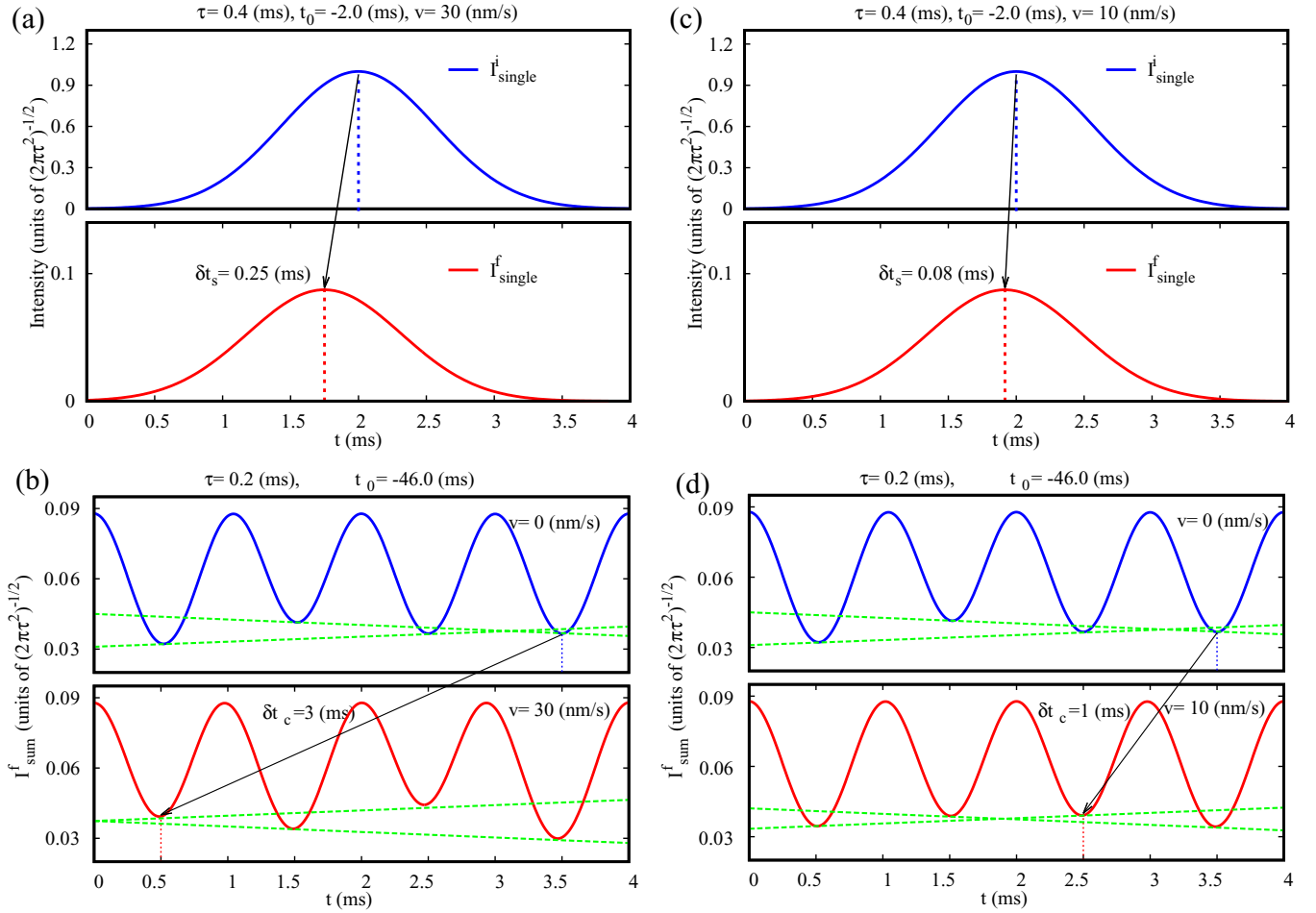


FIG. 5. Numerical simulation of transmission temporal shift of the single Michelson interferometer with $\tau = 0.4$ ms and $t_0 = -2.0$ ms (upper panels) and the two cascaded Michelson interferometers with $\tau = 0.2$ ms and $t_0 = -46.0$ ms (lower panels). For the different measured velocities v , the left panels show the results of the measurement $v = 30$ nm/s, and the right panels display the results of the measurement $v = 10$ nm/s. The unit of the y coordinate of each graph is $(2\pi r\tau^2)^{-1/2}$. Note that the green lines are an additional auxiliary line that we added to determine the position of the characteristic peak.

that our scheme takes more time than that of the single Michelson interferometer, which brings the question of whether our scheme is more sensitive for a given measurement time.

III. FURTHER DISCUSSION AND NUMERICAL RESULTS

A. Sensitivity-enhanced factor at same measurement time

We study the sensitivity-enhanced factor in the two schemes mentioned above at the same measurement time. Note that we can obtain the temporal shift in a certain effective time window, and the rest of the time window is useless in the measurement. For example, when the time is greater than 2 ms in the window in Fig. 4(a), the measurement is invalid.

By choosing the appropriate meter in the TWVA and MWVA techniques, we compare their sensitivity at the same measurement time. Note that we can obtain the temporal shift in a certain and effective time window. The simulation is shown in Fig. 5. I_u^i and I_d^i are chosen for postselection phase $\phi = 0.3$ rad, the length of the individual Gaussian pulse is $\tau = 0.2$ ms, $t_0 = 46.0$ ms of pulses I_u^i (11) and I_d^i (12),

$\bar{R}_{\text{fixed}} = 2.0$ ms, and $\bar{R}_{\text{sliding}} = 1.96$ ms. Then

$$I_d^i = \begin{cases} \sum_{m=0}^N \frac{1}{\sqrt{2\pi \times 0.2^2}} e^{-(t+46-2.00m)^2/(2 \times 0.2^2)} & t < 4 \text{ ms} \\ 0 & t > 4 \text{ ms}, \end{cases}$$

$$I_d^i = \begin{cases} \sum_{m=0}^N \frac{1}{\sqrt{2\pi \times 0.2^2}} e^{-(t+46-1.96m)^2/(2 \times 0.2^2)} & t < 4 \text{ ms} \\ 0 & t > 4 \text{ ms}. \end{cases}$$

To keep the same measurement time, the meter mode I_{single}^i (2) of the schematic of the TWVA technique with the single Michelson in Fig. 1 should be modulated with length $\tau = 0.4$ ms and length $t_0 = -2.0$ ms of the Gaussian pulse. I_{single}^i is given by

$$I_d^i = \begin{cases} \frac{1}{\sqrt{2\pi \times 0.4^2}} e^{-(t-2.0)^2/(2 \times 0.4^2)} & t < 4 \text{ ms} \\ 0 & t > 4 \text{ ms}. \end{cases}$$

With the input of I_{single}^i of the single Michelson in Fig. 1, we can obtain the final meter I_{single}^f (7) of measuring velocity $v = 30$ nm/s and $v = 10$ nm/s in Figs. 5(a) and 5(c). Under the

same window of measurement time, the results of the detected intensity I_{sum}^f of the two cascaded Michelson interferometers measuring velocity $v = 30$ nm/s and $v = 10$ nm/s based on the Vernier effect are as shown in Figs. 5(b) and 5(d).

The method of choosing the window of measurement time is explained as follows: The goal is to obtain the envelope through movement of I_{sum}^f within the smallest possible measurement time window. In our work, we find that the intersection of straight lines determined by the interval troughs can track the shift of the envelope trough. More specifically, the shift of I_{sum}^f can be calculated by tracking the shift of the trough, which is the nearest wave to the right of the intersection. Therefore, we call the above method the intersecting-point-tracing (IPT) method, by which we obtain the shifts of the envelope I_{sum}^f at measuring velocity $v = 30$ nm/s and $v = 10$ nm/s based on the Vernier effect, as shown in Figs. 5(b) and 5(d), respectively. The results show that the IPT method is effective and convenient for tracking the shifts.

From Figs. 5(a) and 5(c), we can obtain the effective sensitivity-enhanced factor of measuring velocity $v = 30$ nm/s, $\bar{E}_m = \frac{3.00 \text{ ms}}{0.25 \text{ ms}} = 12$. From the temporal shifts of measuring velocity $v = 10$ nm/s in Fig. 5(b) and Fig. 5(d), we obtain the same result, $\bar{E}_m = \frac{1.00 \text{ ms}}{0.08 \text{ ms}} = 12$. Although $\bar{E}_m = 12$ is smaller than $\bar{E} = 50$, as calculated from Eq. (10), the sensitivity of the TWVA technique is still enhanced by several orders of magnitude thanks to the Vernier effect.

In the actual measurement process, for the temporal shift to be measurable, we require that $\delta t > \Delta t$, where Δt is the resolution of the detector. In this work, we assume that the shift $\delta t = 0.08$ ms in Fig. 5(c) has reached the resolution Δt , which cannot be measured by the instrument. However, $\delta t = 1.0$ ms $>$ Δt in Fig. 5(d) can be effectively measured due to the enhanced sensitivity of the Vernier effect. Therefore, the MWVA technique based on the Vernier effect can break through the resolution of the detector of the TWVA technique for velocity measurements.

B. Analysis of signal-to-noise ratio based on Fisher information

By calculating the Cramér-Rao bound (CRB) [41,42], we consider the fundamental limitation of velocity measurements with both the traditional WVA technique and the modified WVA technique based on the Vernier effect. The CRB is the fundamental limit of the minimum uncertainty for parameter estimation and is equal to the inverse of the Fisher information. In information theory, the Fisher information is a way of measuring the amount of information that an observable random variable x carries about an unknown parameter Ω upon which the probability of x depends. Let $\mathbf{P}(x|\Omega)$ be the probability density function for x conditioned on the value of Ω . The Fisher information [37] is usually defined as

$$\mathbf{F}(\Omega) = N \int dx \mathbf{P}(x|\Omega) \left[\frac{d}{d\Omega} \ln \mathbf{P}(x|\Omega) \right]^2, \quad (15)$$

where N represents that N photons are sent through the interferometer. Then the CRB, which is the minimum variance $\Delta^2(\Omega)$ of an unbiased estimate of Ω , can be obtained as $\text{CRB} = 1/\mathbf{F}(\Omega)$. We calculate CRB and the SNR for TWVA and MWVA based on the Vernier effect at the same

measurement time, $0 < t < 4$ ms (discussed in Sec. III A). In our work, Ω corresponds to the temporal shift δt .

In the scheme of Fig. 1, with the traditional WVA technique, we choose the pulse in Sec. III A and obtain the probability distribution of t ,

$$\mathbf{P}_s = \begin{cases} \frac{(\sin\phi)^2}{\sqrt{0.32\pi}} e^{-(t-2.0+\delta t)^2/0.32} & t < 4 \text{ ms} \\ 0 & t > 4 \text{ ms}, \end{cases}$$

and the Fisher information can be computed as

$$\mathbf{F}_s = N \int dt \mathbf{P}(t|\delta t) \left[\frac{d}{d\delta t} \ln \mathbf{P}_s(t|\delta t) \right]^2. \quad (16)$$

The sensitivity in the determination of $\delta t = \frac{4\pi\tau^2v}{\lambda\phi}$ is bounded by the square root of the minimum variance, $\Delta(\delta t) = \sqrt{1/\mathbf{F}_s}$. The smallest resolvable velocity is determined by

$$\text{SNR}_s = \frac{\delta t_s}{\Delta(\delta t)} = \frac{v}{\Delta v} = \frac{4v\pi\tau^2\sqrt{\mathbf{F}_s}}{\lambda\phi}, \quad (17)$$

where $\delta t_s = \delta t$.

Figure 3 shows the Fisher information \mathbf{F}_c with the MWVA technique based on the Vernier effect. To keep the same measurement times with the TWVA technique, we choose inputs I_u^i (11) and I_d^i (13) with the parameters in Sec. III A, and the Fisher information \mathbf{F}_c can be calculated as

$$\mathbf{F}_c = N \int dt \mathbf{P}(t|\delta t) \left[\frac{d}{d\delta t} \ln \mathbf{P}_c(t|\delta t) \right]^2, \quad (18)$$

where the probability distribution \mathbf{P}_c satisfies

$$\mathbf{P}_c = \begin{cases} \sum_{m=0}^N \frac{1}{\sqrt{0.08\pi}} [e^{-(t+46-2.00m+\delta t)^2/0.08} + e^{-(t+46-1.96m+\delta t)^2/0.08}] & t < 4 \text{ ms} \\ 0 & t > 4 \text{ ms}. \end{cases}$$

Therefore,

$$\text{SNR}_c = \frac{\delta t_c}{\Delta(\delta t)} = \frac{12v}{\Delta v} = \frac{48v\pi\tau^2\sqrt{\mathbf{F}_s}}{\lambda\phi}, \quad (19)$$

where $\delta t_c = 12\delta t$. Note that SNR_c with the TWVA technique will be enhanced with the factor $\bar{E}_m = 12$ due to the Vernier effect.

The complexity of probability distributions \mathbf{P}_s and \mathbf{P}_c makes it difficult to analytically calculate the Fisher information. We numerically perform the integrations (16) and (18) for $N = 54 \times 10^6$, with results as shown in Fig. 6(a). On this basis, we calculate the SNR at different velocities with the TWVA and MWVA techniques. Accordingly, these results are shown in Fig. 6(b).

The CRB [41,42] states that the inverse of the Fisher information is a lower bound on the variance of any unbiased estimator of δt . $\Delta^2(\delta t)$ represents the noise limit of the measurement process and characterizes the extent of the shot noise of the quantum measurement [22]. The Fisher information intuitively reflects the accuracy of our parameter estimation. The larger it is the greater the accuracy is, i.e., it represents more information. Fig. 6(a) shows that the Fisher information \mathbf{F}_c with MWVA is greater than \mathbf{F}_s with the traditional TWVA when the measured velocity is less than 32 nm/s [read from Fig. 6(a)]. However, with the further increase of velocity v , MWVA will become less efficient than TWVA. As we have pointed out, MWVA is an effective alternative to TWVA when

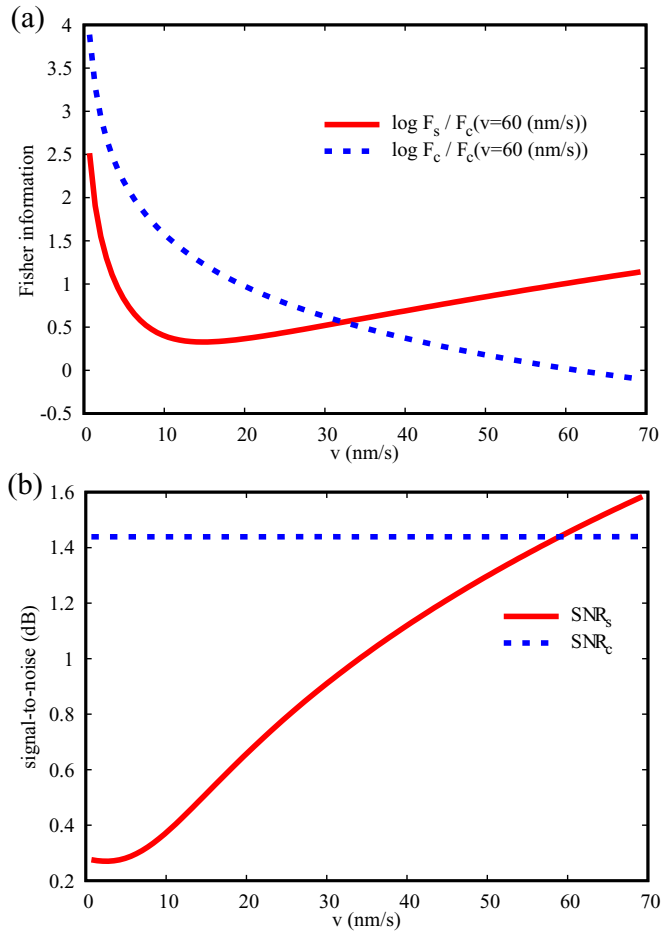


FIG. 6. (a) Fisher information and (b) SNR at different velocities with traditional WVA technique and modified WVA technique based on Vernier effect.

the measurement is beyond the limits of resolution of the detector in Fig. 1.

Continuing the discussion of the SNR in Fig. 6(b), the results show that SNR_c is greater than SNR_s with the traditional WVA technique when our measured velocity is less than 58 nm/s [read from Fig. 6(b)]. Note that an interesting conclusion can be drawn from Fig. 6. The Fisher information characterization is not fully equivalent to the SNR characterization with the increase of measurement velocity. A similar conclusion is obtained by analyzing the WVA technique beyond the Aharonov-Albert-Vaidman limit [22]. In addition, as the measurement velocity decreases, the SNR of MWVA improves more.

We notice that the time shift δt_c in our MWVA technique is less than 3.5 ms, thanks to the same time measurement window being guaranteed. The upper limit of the corresponding velocity measurement is 40 nm/s. Therefore, we can conclude that MWVA is more efficient than TWVA because SNR_c is larger than SNR_s , as $v < 40$ nm/s in Fig. 6(b). In addition, the MWVA technique shows its advantage of the enhanced sensitivity and the higher SNR when the velocity measurement is smaller especially when the TWVA technique loses the sensitivity (where δt is smaller than the resolution of the detector).

IV. SUMMARY AND DISCUSSION

Using the feature of sensitivity enhancement in the Vernier effect, we proposed the modified weak-value-amplification technique to measure the mirror's velocity. Compared with the traditional weak-value-amplification, we demonstrated a sensitivity-enhanced and higher signal-to-noise ratio (SNR) by using two cascaded Michelson interferometers with similar optical structures. An interferometer with a fixed mirror acts as a fixed part of the Vernier scale, and the other, with a moving mirror, acts as a sliding part of the Vernier scale for velocity sensing. By choosing the appropriate meter in modified weak-value-amplification and traditional weak-value-amplification to ensure the same measurement time. Our numerical results showed that modified weak-value-amplification is more efficient than the traditional technique, with 12 times sensitivity enhancement and a higher signal-to-noise ratio. In addition, as the measurement velocity is smaller, the signal-to-noise ratio of modified weak-value-amplification is improved more. Note that modified weak-value-amplification can present a viable and effective alternative to the measurement out of the limit of resolution in the traditional weak-value-amplification technique.

A few remarks are warranted. We proposed an intersecting point-tracking (IPT) method to track the shift of the meter with cascaded Michelson interferometers, which indicates that the intersection of straight lines determined by interval troughs can track the shift of the envelope trough. We found that Fisher information characterization is not fully equivalent to signal-to-noise ratio characterization with the increase of measurement velocity. A similar result can be found in Ref. [22]. Our study can serve as a purely theoretical discussion of this inconsistency among Fisher information and signal-to-noise ratio. In addition, by using the principles of the Vernier effect, it is applicable and convenient to further improve the sensitivity and signal-to-noise ratio in measuring other physical quantities with the weak-value-amplification technique.

Note that our modified weak-value amplification is only one of the techniques used in precision interferometric measurements. There are lots of effective efforts that may be able to be combined with our scheme as well. For example, we could map our system to a Fabry-Pérot cavity [31], which could improve the sensitivity without postselection by changing the finesse of the cavity. Future work may focus on the combination of this technique and our work. In addition, our modified weak-value-amplification technique can be realized beyond the Gaussian meter wave function. It has been shown [43] that the Hermite-Gaussian and Laguerre-Gaussian pointer states for a given coupling direction have advantages and disadvantages compared with the fundamental Gaussian mode in improving the signal-to-noise ratio, and it has been indicated [44] that the postselected weak measurement scheme for nonclassical pointer states (coherent, squeezed vacuum, and Schrödinger cat states) is superior to semiclassical schemes. Therefore, a modified weak-value-amplification technique with a non-Gaussian meter wave function based on the Vernier effect will be studied in our future work, whose relevant experiments are gradually being carried out.

ACKNOWLEDGMENTS

This study is financially supported by MOST Special Fund from the State Key Laboratory of Geological Processes

and Mineral Resources, China University of Geosciences (No. MSFGPMR01-4) and the Fundamental Research Funds for National Universities, China University of Geosciences (Wuhan) (Grant No. G1323519204).

-
- [1] F. Lecocq, L. Ranzani, G. A. Peterson, K. Cicak, X. Y. Jin, R. W. Simmonds, J. D. Teufel, and J. Aumentado, Efficient Qubit Measurement with a Nonreciprocal Microwave Amplifier, *Phys. Rev. Lett.* **126**, 020502 (2021).
- [2] J. T. Monroe, N. Y. Halpern, T. Lee, and K. W. Murch, Weak Measurement of a Superconducting Qubit Reconciles Incompatible Operators, *Phys. Rev. Lett.* **126**, 100403 (2021).
- [3] Y. Aharonov, D. Z. Albert, and L. Vaidman, How the Result of a Measurement of a Component of the Spin of a Spin-1/2 Particle Can Turn Out to be 100, *Phys. Rev. Lett.* **60**, 1351 (1988).
- [4] Y. Aharonov and L. Vaidman, Aharonov and Vaidman Reply, *Phys. Rev. Lett.* **62**, 2327 (1989).
- [5] A. Peres, Quantum Measurements with Postselection, *Phys. Rev. Lett.* **62**, 2326 (1989).
- [6] A. J. Leggett, Comment on “How the Result of a Measurement of a Component of the Spin of a Spin-(1/2 Particle Can Turn out to Be 100”, *Phys. Rev. Lett.* **62**, 2325 (1989).
- [7] L. Vaidman, Lorentz-Invariant “Elements of Reality” and the Joint Measurability of Commuting Observables, *Phys. Rev. Lett.* **70**, 3369 (1993).
- [8] J. S. Lundeen and A. M. Steinberg, Experimental Joint Weak Measurement on a Photon Pair as a Probe of Hardy’s Paradox, *Phys. Rev. Lett.* **102**, 020404 (2009).
- [9] K. Yokota, T. Yamamoto, M. Koashi, and N. Imoto, Direct observation of Hardy’s paradox by joint weak measurement with an entangled photon pair, *New J. Phys.* **11**, 033011 (2009).
- [10] Y. Aharonov and L. Vaidman, Complete description of a quantum system at a given time, *J. Phys. A: Math. Gen.* **24**, 2315 (1991).
- [11] K. Resch, J. Lundeen, and A. Steinberg, Experimental realization of the quantum box problem, *Phys. Lett. A* **324**, 125 (2004).
- [12] D. Rohrlich and Y. Aharonov, Cherenkov radiation of superluminal particles, *Phys. Rev. A* **66**, 042102 (2002).
- [13] A. Weissberger and B. W. Rossiter, Spectroscopy and spectrometry in the infrared, visible, and ultraviolet, *Nature (London)* **474**, 188 (2011).
- [14] A. Szorkovszky, A. C. Doherty, G. I. Harris, and W. P. Bowen, Mechanical Squeezing Via Parametric Amplification and Weak Measurement, *Phys. Rev. Lett.* **107**, 213603 (2011).
- [15] O. S. Magaña-Loaiza, M. Mirhosseini, B. Rodenburg, and R. W. Boyd, Amplification of Angular Rotations Using Weak Measurements, *Phys. Rev. Lett.* **112**, 200401 (2014).
- [16] G. Li, T. Wang, and H.-S. Song, Amplification effects in optomechanics via weak measurements, *Phys. Rev. A* **90**, 013827 (2014).
- [17] L. Luo, Y. He, X. Liu, Z. Li, P. Duan, and Z. Zhang, Anomalous amplification in almost-balanced weak measurement for measuring spin hall effect of light, *Opt. Express* **28**, 6408 (2020).
- [18] J. H. Huang, X.-Y. Duan, and X.-Y. Hu, Amplification of rotation velocity using weak measurements in Sagnac’s interferometer, *Eur. Phys. J. D* **75**, 114 (2021).
- [19] P. B. Dixon, D. J. Starling, A. N. Jordan, and J. C. Howell, Ultrasensitive Beam Deflection Measurement via Interferometric Weak Value Amplification, *Phys. Rev. Lett.* **102**, 173601 (2009).
- [20] G. I. Viza, J. Martínez-Rincón, G. A. Howland, H. Frostig, I. Shomroni, B. Dayan, and J. C. Howell, Weak-values technique for velocity measurements, *Opt. Lett.* **38**, 2949 (2013).
- [21] A. K. Pati, C. Mukhopadhyay, S. Chakraborty, and S. Ghosh, Quantum precision thermometry with weak measurements, *Phys. Rev. A* **102**, 012204 (2020).
- [22] J. Ren, L. Qin, W. Feng, and X.-Q. Li, Weak-value-amplification analysis beyond the Aharonov-Albert-Vaidman limit, *Phys. Rev. A* **102**, 042601 (2020).
- [23] S. Pang and T. A. Brun, Improving the Precision of Weak Measurements by Postselection Measurement, *Phys. Rev. Lett.* **115**, 120401 (2015).
- [24] T. Koike and S. Tanaka, Limits on amplification by Aharonov-Albert-Vaidman weak measurement, *Phys. Rev. A* **84**, 062106 (2011).
- [25] S. Pang, T. A. Brun, S. Wu, and Z.-B. Chen, Amplification limit of weak measurements: A variational approach, *Phys. Rev. A* **90**, 012108 (2014).
- [26] D. J. Starling, P. B. Dixon, A. N. Jordan, and J. C. Howell, Optimizing the signal-to-noise ratio of a beam-deflection measurement with interferometric weak values, *Phys. Rev. A* **80**, 041803(R) (2009).
- [27] A. Feizpour, X. Xing, and A. M. Steinberg, Amplifying Single-Photon Nonlinearity Using Weak Measurements, *Phys. Rev. Lett.* **107**, 133603 (2011).
- [28] J. Huang, Y. Li, C. Fang, H. Li, and G. Zeng, Toward ultra-high sensitivity in weak-value amplification, *Phys. Rev. A* **100**, 012109 (2019).
- [29] C. Krafczyk, A. N. Jordan, M. E. Goggin, and P. G. Kwiat, Enhanced Weak-Value Amplification Via Photon Recycling, *Phys. Rev. Lett.* **126**, 220801 (2021).
- [30] B. de Lima Bernardo, Photon statistics as a probe for weak measurements, *J. Opt. Soc. Am. B* **31**, 1494 (2014).
- [31] S. Carrasco and M. Orszag, Weak-value amplification of photon-number operators in the optomechanical interaction, *Phys. Rev. A* **99**, 013801 (2019).
- [32] O. S. Magaña-Loaiza *et al.*, Multiphoton quantum-state engineering using conditional measurements, *npj Quantum Inf.* **5**, 80 (2019).
- [33] D. Dai, Highly sensitive digital optical sensor based on cascaded high- Q ring-resonators, *Opt. Express* **17**, 23817 (2009).
- [34] T. Claes, W. Bogaerts, and P. Bienstman, Experimental characterization of a silicon photonic biosensor consisting of two cascaded ring resonators based on the vernier-effect and introduction of a curve fitting method for an improved detection limit, *Opt. Express* **18**, 22747 (2010).

- [35] H. H. Zhu, Y. H. Yue, Y. J. Wang, M. Zhang, L. Y. Shao, J. J. He, and M. Y. Li, High-sensitivity optical sensors based on cascaded reflective MZIs and microring resonators, *Opt. Express* **25**, 28612 (2017).
- [36] Y. Liu, Y. Li, M. Li, and J.-J. He, High-sensitivity and wide-range optical sensor based on three cascaded ring resonators, *Opt. Express* **25**, 972 (2017).
- [37] H. M. Wiseman and G. J. Milburn, *Quantum Measurement and Control* (Cambridge University Press, Cambridge, 2009).
- [38] N. Brunner and C. Simon, Measuring Small Longitudinal Phase Shifts: Weak Measurements or Standard Interferometry?, *Phys. Rev. Lett.* **105**, 010405 (2010).
- [39] L.-Y. Shao, Y. Luo, Z. Zhang, X. Zou, B. Luo, W. Pan, and L. Yan, Sensitivity-enhanced temperature sensor with cascaded fiber optic Sagnac interferometers based on vernier-effect, *Opt. Commun.* **336**, 73 (2015).
- [40] S. Zeng, K. Bi, S. Xue, Y. Liu, X. Lv, and Q. Luo, Acousto-optic modulator system for femtosecond laser pulses, *Rev. Sci. Instrum.* **78**, 15103 (2007).
- [41] B. R. Frieden and R. A. Gatenby, Principle of maximum Fisher information from Hardy's axioms applied to statistical systems, *Phys. Rev. E* **88**, 042144 (2013).
- [42] T. Pfister, A. Fischer, and J. Czarske, Cramér-Rao lower bound of laser Doppler measurements at moving rough surfaces, *Meas. Sci. Technol.* **22**, 055301 (2011).
- [43] Y. Turek, H. Kobayashi, T. Akutsu, C.-P. Sun, and Y. Shikano, Post-selected von Neumann measurement with hermite-Gaussian and Laguerre-Gaussian pointer states, *New J. Phys.* **17**, 083029 (2015).
- [44] Y. Turek, W. Maimaiti, Y. Shikano, C.-P. Sun, and M. Al-Amri, Advantages of nonclassical pointer states in postselected weak measurements, *Phys. Rev. A* **92**, 022109 (2015).